Ice-Templated Materials: Sophisticated Structures Exhibiting Enhanced Functionalities Obtained after Unidirectional Freezing and Ice-Segregation-Induced Self-Assembly†

María C. Gutiérrez, María L. Ferrer, and Francisco del Monte*

Instituto de Ciencia de Materiales de Madrid (ICMM), Consejo Superior de Investigaciones Científicas (CSIC), Cantoblanco 28049, Madrid, Spain

Received July 26, 2007. Revised Manuscript Received November 12, 2007

This review aims to demonstrate the capability of the ice-segregation-induced self-assembly (ISISA) process for the preparation of materials with highly sophisticated structures (e.g., hierarchical materials exhibiting organization at different scale levels). Cryogenic processes (consisting of the freezing, storage in the frozen state for a definite time, and defrosting of low - or high-molecular-weight precursors, as well as colloid systems, as either a water solution or suspension, or forming a hydrogel) have been widely used for the scaffolds preparation. However, the recent success in the control of the morphology (e.g., by unidirectional freezing in nitrogen liquid) and the possibility to extend the compositional nature of the resulting materials has recently attracted much attention to the ISISA process. Besides, this review aims to exemplify how the aqueous nature of the ISISA process allows for the in-situ incorporation of biological entities which provides not only hierarchy but also functionality to the resulting materials. The combination of hierarchy and functionality is characteristic of biological structures and must make these "smart" materials highly suitable in biotechnology and biomedicine. Thus, interesting examples of biocatalytic materials (for organic synthesis and fuel cell technologies) and biosensors, and scaffolds exhibiting enhanced functional (in terms of both biocompatibility and biodegradability) and mechanical performance, are reviewed in this work.

Introduction

Nanochemistry aims to extend the traditional length scales of synthetic chemistry and exploit the collective properties of organized assemblies.[1] Structurally organized inorganic materials[2] have attracted much attention for emerging applications (e.g., catalysis, storage and controlled release systems, smart fillers, and biotechnologies) given that they offer a desirable combination of an extensive internal reactive surface along narrow nanopores with facile molecular transport through broad "highways" leading to and from these pores.[3]

Inorganic materials, although diverse in composition, generally lack the structural variety of supramolecular and other organic structures.[4] The discovery of mesoporous silica materials[5] formed by using organic compounds (e.g., molecular, supramolecular, or colloidal crystalline) as templates was a breakthrough in the design of strategies for the preparation of well-organized inorganic and hybrid materials.[6] Thus, the imprinting of an inorganic structure from an organic one has been achieved for a variety of organic templates, resulting in materials whose shape is controlled at both the microscopic and the nanoscopic level. Lately, an increased degree of sophistication has even been attained by the use of chiral organic templates that result in the formation of their inorganic chiral counterparts.[7] Attempts have also been made to reproduce biological structures that, besides functionality, offer organization across a large range of length scales. The rich variety of forms found in biological species provides many possible structures suitable for imitation. Silica transcription has proved an ideal approach to structure replication,[8] and there is quite a list of biological forms which may be used as templates. Among others, pine and poplar wood,[9] diatoms,[10] various cellulose-based substances,[11] eggshell membranes,[12] spider silk fibers,[13] insect wings,[14] pollen grains,[15] and cuttlebones[16] are representative examples. Transcription for preparation of complex structured materials with different levels of space organization (e.g., hierarchy materials) is currently a common research topic of a number of groups.[17] However, the success of these routes in the reproduction of natural structures has only been partial, given the morphological complexity with sophisticated levels of structure organization, from the macroscale all the way through to the nanoscale, of such structures.

In occasions, synthetic alternatives to transcription are required to obtain a structure of the required sophistication. The combined use of different templates has recently allowed for the achievement of bimodal and even trimodal pore structured materials, in spite of the intrinsic difficulty that implies the preservation of the existing levels of organization when a further one is introduced.[18] Template removal (e.g., by thermal or dissolution treatments) yields a hierarchically organized material with a structure that is a replica of that of the original template. However, despite the widespread use of these processes, the achievement of hierarchical biohybrid materials is rare. The reasons for this most likely

† Part of the "Templated Materials Special Issue".

* Corresponding author. E-mail: delmonte@icmm.csic.es.

10.1021/cm702028z CCC: $40.75
Published on Web 01/04/2008

reside in the chemical nature of the templates and/or the processes used for their removal which, in practice, have mainly limited the composition of the resulting bimodal/trimodal pore structures to inorganic ones. It is noted that the use of biological molecules and structures (e.g., proteins and liposomes, respectively) as templates would provide materials with not only increased levels of space organization but also functionalities, i.e., smart biocatalytic and drug delivery systems, among others. Thus, there is currently a continuing need for novel fabrication methodologies (e.g., synthesis in ionic liquids)[19] as well as for materials with increased levels of spatial organization and functionalities.[20]

In view of the huge time frame that nature has had to optimize and perfect functional materials, it is not surprising that imitation of nature in materials preparation has caught the attention of numerous research groups aiming to obtain complex and functional hierarchically organized chemical structures.[21] If one desires to imitate nature when synthesizing complex structures, one is inevitably led to consider processes involving water as solvent. Water is one of the most common chemical substances on our blue planet (it covers ca. 71% of the surface of the earth) and is essential to all known forms of life, from the most simple bacteria and other microorganisms to the most complex higher organisms.[22] Moreover, water solutions provide a friendly environment for functional templates both natural and synthetic (e.g., micelles, vesicles, liposomes, low molecular weight gelators (LMWG), proteins, and cell membranes, among others), in which the complex structure of these templates (i.e., supramolecular for LMWG or tertiary/quaternary for proteins) is stable. Thus, it is our belief that the design of "aqueous processes" capable of introducing further levels of spatial organization, while preserving those that already exist, would be of tremendous interest for the preparation of complex and functional hierarchically organized structures.

Ice-Templating Process for Preparation of Well-Ordered Macrostructures

1. Origin of Cryogels: Polymers and Ceramics. A close inspection of the bibliography allows one to point to cryogenic processes as excellent candidates for the purpose of templating. Cryogenic processes consist of the freezing, storage in the frozen state for a certain time, and defrosting (simple thawing or freeze-drying) of low- or high-molecular-weight precursors as well as colloid systems, forming either a water solution or suspension or a hydrogel. Thus, the formation of crystalline ice (hexagonal ice, typically) causes every solute originally dispersed in the aqueous medium to be expelled to the boundaries between adjacent ice crystals (Figure 1). Subsequent freeze-drying (high-vacuum sublimation of ice) gives rise to a cryogel, whose name derives from the Greek κριοσ (kryos) meaning frost or ice. Cryogels are macroporous structures characterized by "walls" of matter enclosing empty areas where ice crystals originally resided. The freeze-drying process also allows for the achievement of monoliths that preserve the size and shape of the container submitted to freezing (Figure 2). Cryogels of polymeric nature were first reported more than 40 years ago,[23,24] and

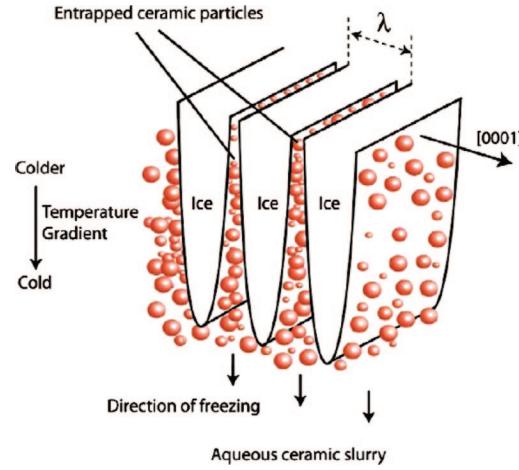

Figure 1. Pattern formation and particle segregation during freeze-casting of ceramic slurries. The ice platelets grow in a direction perpendicular to the *c*-axis of hexagonal ice. The interlamellar separation of the structure is represented by λ. Reprinted with permission from ref 38d. Copyright 2007 Elsevier.

their properties, rather unusual for polymer gels, soon attracted attention. Since then, polymer cryogels of many different compositions (e.g., poly(L-lactic acid) and poly(DL-lactic-*co*-glycolic acid),[25,26] gelatin,[27] g-PGA/chitosan,[27–29] collagen and elastin,[30] collagen−glycosaminoglycan,[31] or albumin-cross-linked polyvinylpyrrolidone (PVP) hydrogels,[32] among others) have been widely used in biomedicine (e.g., for tissue engineering and drug delivery purposes) most likely because of the biocompatible character of the process. It is noted that the process start from an aqueous solution/suspension or from a hydrogel and proceed in the absence of further chemical reactions or purification procedures, thus avoiding potential medical complications which might be associated with byproduct or with the removal of templates. Cryogels of ceramic nature (in particular, bundles of aligned silica fibers)[33] were first reported later on by Mahler and Bechtold, in 1980, their production being based on previous studies of freeze-drying techniques for the synthesis of metal and metal oxide powders.[34–36] Since 1980, numerous works (albeit less than for polymers) have also reported ice-templating processes for preparation of different porous ceramic materials; alumina bodies with a uniform microstructure, for example, have been obtained by freeze-casting slurries of water and water/glycerol solutions containing high loadings of alumina.[37]

2. Cryogels with Controlled Morphology: Ceramics and Carbon Composites. In spite of the common application of cryogenic processes for the preparation of ceramic and polymer scaffolds, control of scaffold morphology was only partial. More recently, though, a number of workers have demonstrated the capacity of ice-templating processes to control the morphology of the resulting macroporous structures by the use of unidirectional freezing at a controlled immersion rate.[38] Unidirectional freezing allows for the achievement of microchanneled structures well-aligned in the freezing direction (see longitudinal view in Figure 2) with a well-patterned between-channel morphology (e.g., microhoneycomb or lamellar, among others; see cross-sectional

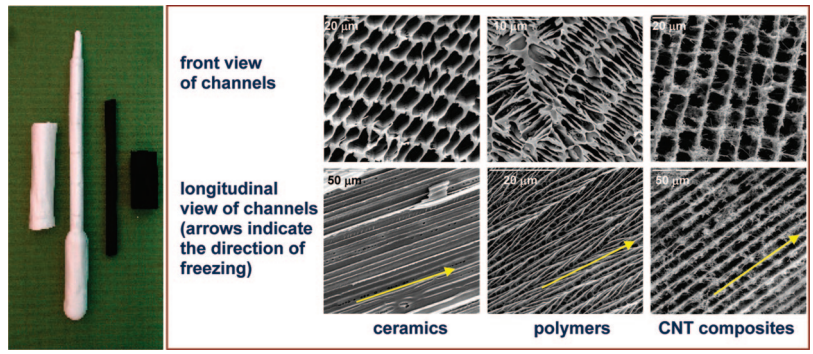

Figure 2. Left: monolithic cryogels of different nature, and different sizes and shapes, obtained by ice-templating processes (from left to right: ceramics, polymers, and CNT composites). Right: SEM micrographs of cross and longitudinal sections of well-patterned microchanneled materials of different natures (ceramics, polymers, and CNT composites) formed by ice-templating processes. The micrographs of polymers and CNT composites are from refs 56, 66, and 75. Copyright 2007 American Chemical Society, Royal Society of Chemistry and Wiley-VCH.

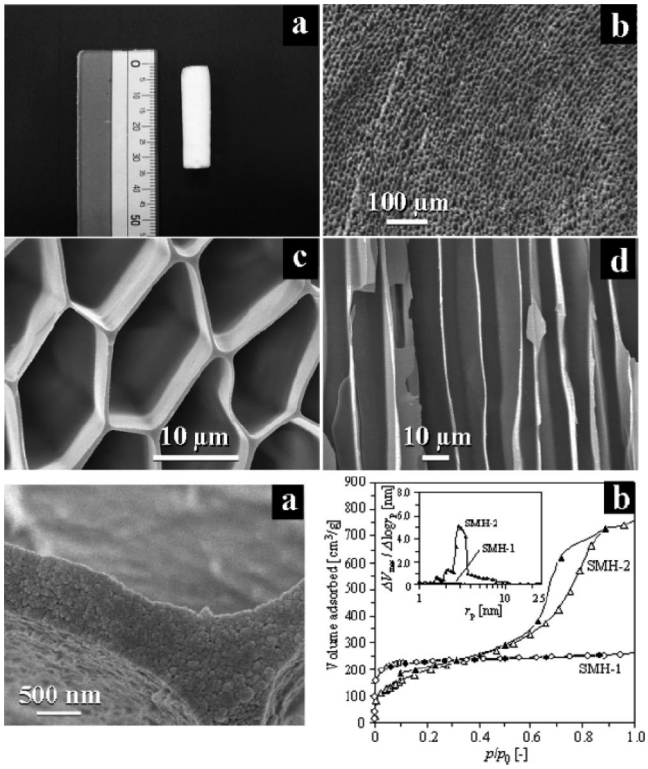

Figure 3. Morphology and structure of silica monoliths exhibiting a micro-honeycomb structure. Upper: (a) An overall image. SEM images of (b) cross section, (c) microchannel structure, and (d) longitudinal section. Lower (a) Detail of a cross section. Nitrogen isotherms (b) are also represented. The inset shows the mesopore size distribution in the desorption branches. Reprinted with permission from ref 38a. Copyright 2004 Royal Society of Chemistry.

views in Figure 2). Moreover, these workers have extended the use of this process for preparation of materials of different compositions (phenolic resins and colloidal silica).[39] This feature allowed Tamon and co-workers to create silica monoliths that were not only macroporous (the cell size of the micro-honeycomb structure ranges between 10 and 15 μm) but also meso- and microporous (the BET surface area ranges between 400 and 700 m^2/g).[39] It is noted that the microporosity is simply a consequence of the voids left between silica colloids packaged at the boundaries of adjacent ice crystals (Figure 3). These authors have also prepared macroporous monoliths of $Al_2O_3-SiO_2$ with similar micro-honeycomb structures (macropore sizes ranging from 10 to 20 μm) and microporosity/mesoporosity (BET surface area and pore volume greater than 700 m^2/g and 0.45 cm^3/g, respectively).[40] In this case, the $Al_2O_3-SiO_2$ hydrogels were produced by soft annealing at 303 K of a water dilution of sodium silicate at pH 3 and aluminum nitrate ($Al(NO_3)_3 \cdot 9H_2O$). The distribution of Al atoms throughout the macroporous monoliths was homogeneous (demonstrated by Al mapping analysis using energy dispersive X-ray diffractometry), without local aggregation (which is not necessarily an unequivocal result when working with binary oxides), due to the incorporation of Al atoms into the silica framework by formation of an Al−O−Si polymeric network. Interestingly, the macroporous monoliths exhibit acid sites, allowing this material to be used as a solid acid catalyst.

Tamon and co-workers have also applied this ice-templating process to TiO_2 hydrogels for the preparation of porous titania cryogel fibers (TCFs).[41] TiO_2 hydrogels were synthesized by the polymerization of titanium tetraisopropoxide (TTIP) in an ethanol/water mixture using HCl as the catalyst, followed by dialysis. By adjusting the concentrations of TTIP and replacing the water included in the titania hydrogel fibers with *tert*-butyl alcohol, mesoporous TCFs having a unique fiber morphology were successfully prepared. The crystalline phase of the as-dried TCFs was anatase, and these TCFs had a BET surface area greater than 400 m^2/g. Thermal treatment, at ca. 400 °C, of TCFs yielded a product which exhibited remarkable photocatalytic activity for the decomposition of large organic molecules, in the same activity range as that obtained with Degussa P-25.

The preparation of fibers of carbon composites has also been described by Tamon and co-workers (Figure 4).[39c] In this case, the ice-templating approach was applied to resorcinol−formaldehyde (RF) hydrogels obtained by sol–gel polycondensation of resorcinol with formaldehyde using sodium carbonate (Na_2CO_3) as a basic catalyst. Interestingly, by simply decreasing the aging time of the RF gel prior to freezing, cryogels (with a micro-honeycomb-like macroporous structure similar to those described above) are obtained (macropore sizes ranging from 20 to 50 μm, see Figure 4). The further achievement of high values of mesoporosity (surface areas ranging from 500 to 1200 m^2/g) by submission of the monolith to solvent exchange (with *tert*-butyl alcohol) prior to freeze-drying

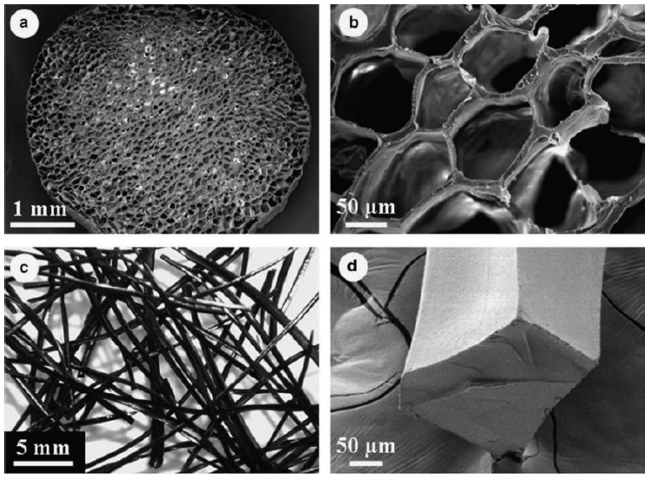

Figure 4. Micro-honeycomb (a, b) or fiber (c, d) structures of ice-templated carbons synthesized by resorcinol−formaldehide hydrolysis and condensation and subsequent carbonization. Reprinted with permission from ref 39c. Copyright 2005 Elsevier.

allowed the authors to obtain hierarchically structured carbons with bimodal porosity at both the macro- and mesoscale.

3. Taking Advantage of the Aqueous Nature of the Process. *3.1. Biohybrids.* In light of the results of Tamon and co-workers, one may propose that the presence in the hydrogel of further and more sophisticated organic assemblies might lead to the formation of structures with increased levels of complexity. Having in mind the above-mentioned stability that water solutions provide to a number of biological molecular assemblies, our group has recently prepared hierarchically organized structures through the application of the ice-templating process (the so-called ISISA, ice-segregation-induced self-assembly) to a silica hydrogel also containing proteins or liposomes (Figures 5 and 6, respectively).[42,43] The former comprised an esterase protein (pig liver esterase, PLE) dispersed in poly(vinyl alcohol) (PVA)/silica hybrid hydrogel which, after ISISA, resulted in a hierarchical biohybrid material exhibiting a very sophisticated structure with up to six levels of space organization, i.e., the ternary structure of PLE, the PVA nanodomains surrounding the esterase, the silica cages entrapping the PVA nanodomains, and the macroporous structure resulting from ISISA. The hybrid nature of the hierarchical material conferred by the PVA nanodomains is ultimately crucial for the preservation of enzyme structure and activity (Figure 5). Furthermore, these hierarchical biohybrid materials show an interesting dual character which allows for sharing of tasks, some entities supporting the structure (e.g., colloidal silica and PVA nanodomains) and others providing functionality (e.g., in this case, PLE). Biohybrid materials which exhibiting fine control over different levels of spatial organization are also of great interest in the fields of chip and sensor technology, catalysis/biocatalysis, and chromatography as well as biomedicine, given the combination of a macroporous structure (allowing efficient mass transport) with a large internal reactive surface area. In particular, the synthesis of pure enantiomers,[44] kinetic

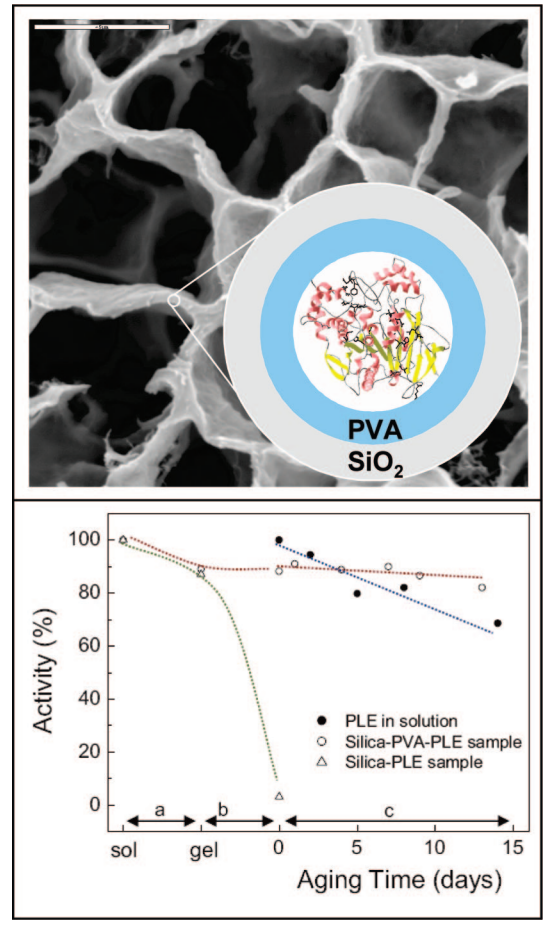

Figure 5. Upper: SEM micrograph and scheme representing PLE encapsulation within the hybrid structure of PVA−silica. The bar is 5 μm long. Lower: evolution of the enzymatic activity of PLE during formation of silica (open triangle, green line) and PVA−silica (open circle, red line) samples: (a) gelation and (b) freeze-drying. (c) Evolution of the enzymatic activity of PLE in solution (solid circle, blue line) and in the PVA−silica sample (open circle, red line), with ageing time. Lines represent a guide for the eye. Reprinted with permission from ref 42. Copyright 2006 Wiley-VCH.

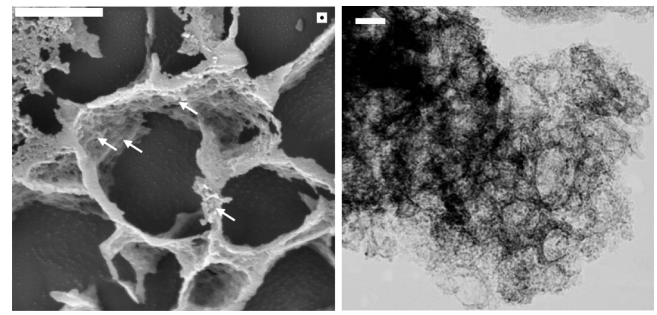

Figure 6. Left: SEM micrographs of the hierarchically organized structure resulting from application of the ice-templating process to silica hydrogel containing liposomes of ~200 nm diameter. The inset at the upper right corner of the left-hand figure represents a sphere of diameter 200 nm. The arrows point to some representative liposomes. The bar is 5 μm long. Right: TEM micrograph of a vacuum-dried hierarchical assembly composed of colloidal silica and dimyristoylphosphatidic acid (DMPA) liposomes. The bar here is 200 nm long. Reprinted with permission from ref 43. Copyright 2006 American Chemical Society.

resolutions, and asymmetric syntheses of organic compounds (e.g., the total synthesis of D-biotin[45]) in continuous flow are reactions of interest to study in these kinds of microchanneled materials.

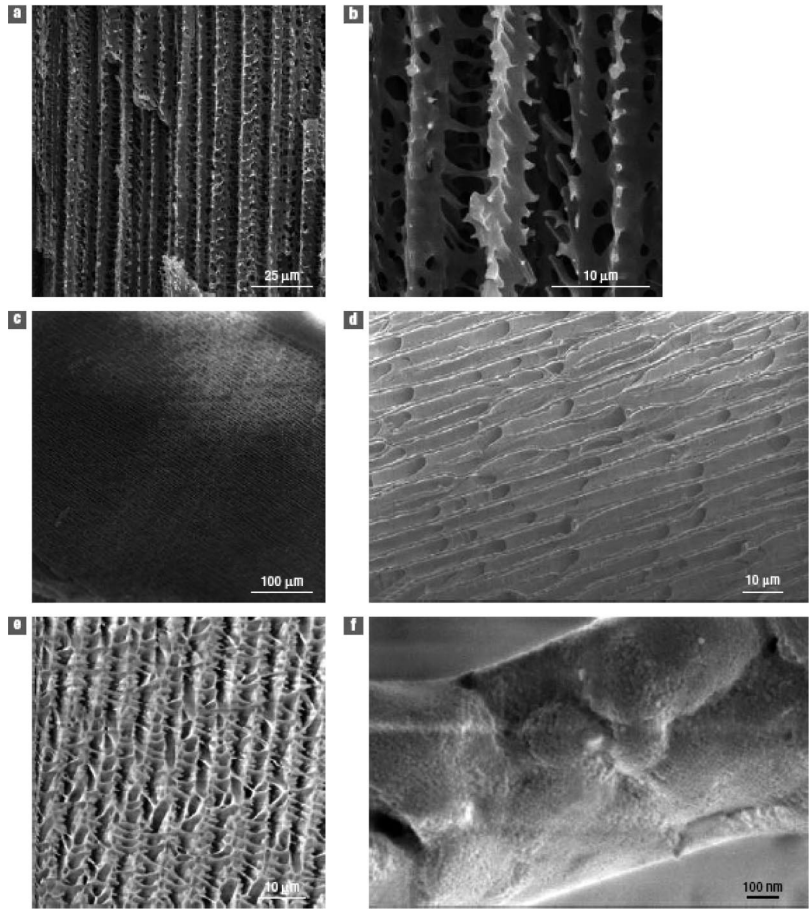

Figure 7. SEM micrographs of (a, b) aligned porous PVA showing pore alignment (a) and the PVA "fish-bone" morphology (b); (c, d) aligned porous PVA−silica composite showing broad alignment of the pore structure (c) and at a higher magnification the parallel channels, each a few micrometers in diameter (d); (e) cross section of the porous PVA−silica composite perpendicular to the direction of alignment; (f) nanoparticulate structure of the composite—the silica particles that make up the structure have an average diameter of 15 nm. Reprinted with permission from ref 48. Copyright 2005 Nature Publishing Group.

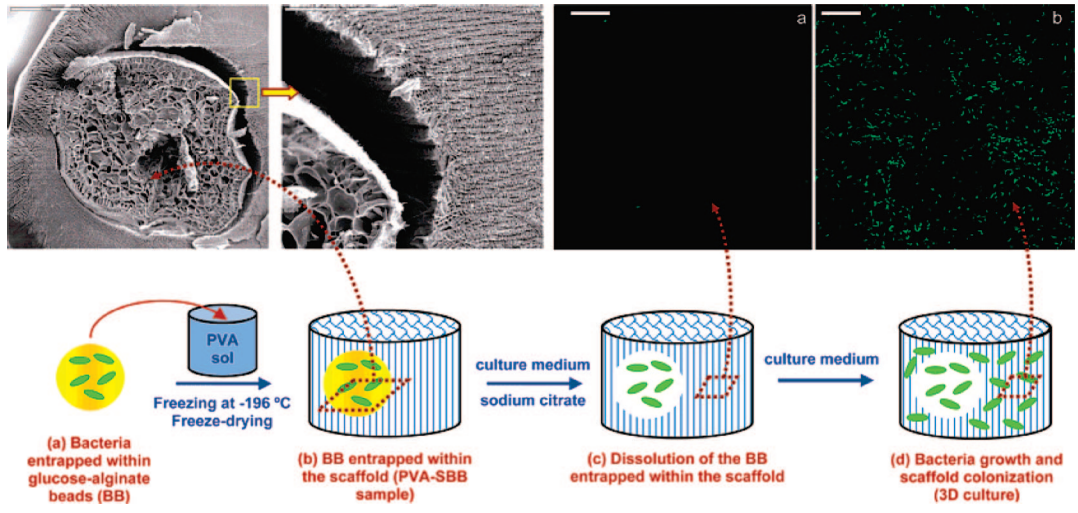

Figure 8. Scheme presenting the process followed for preparation of a PVA scaffold with immobilized bacteria-containing alginate beads. SEM micrographs show a bead of ca. 1 mm entrapped within the microchanneled structure of the PVA scaffold. Scale bars are (left) 500 and (right) 200 μm. Confocal fluorescence microscopic images of the PVA scaffold entrapping bacteria-containing alginate beads soaked in culture medium: (a) before and (b) after incubation at 37 °C for 24 h. Scale bars are 20 μm. Reprinted with permission from ref 49. Copyright 2007 American Chemical Society.

More intriguing is the application of this self-assembly process to gels formed from binary colloidal systems, the term binary applying to both size and composition (Figure 6).[43] For this purpose, our group has studied the assembly formation in binary systems composed of stable liposomes of ~100 nm size dispersed within an aqueous silica gel formed of colloids of ca. 40 nm. The hierarchical assembly resulting after ice templating (with up to five levels of space organization) resembles tessellated liposomes "surface decorating" multiple and interconnected silica fences. Remarkably, the liposomes retain their reversible phase transition (hence the functionality) regardless of their integration within

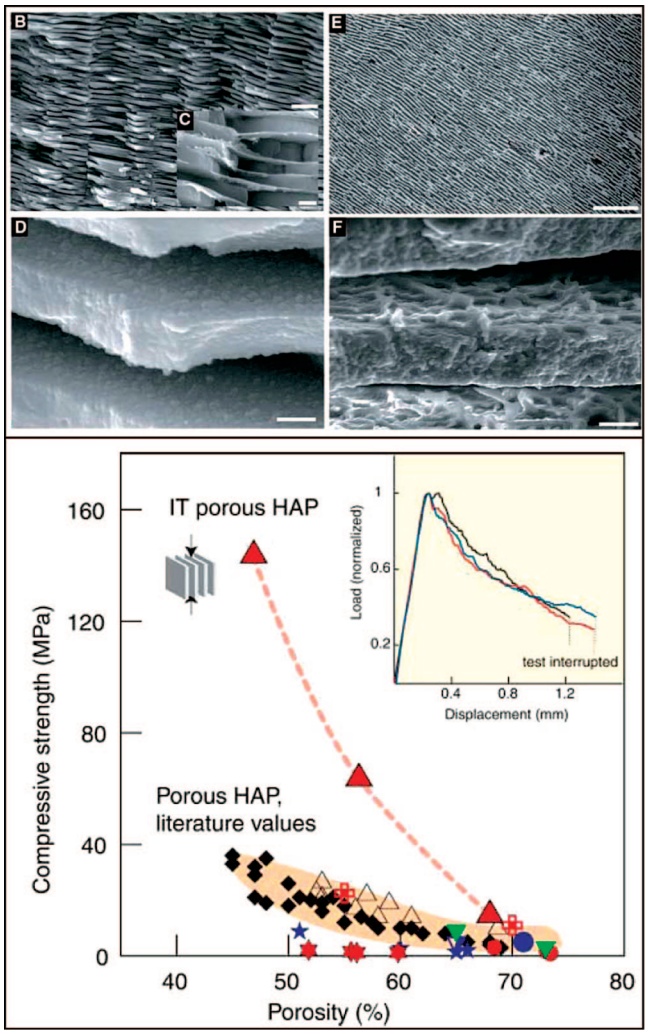

Figure 9. Upper: SEM micrographs of natural nacre (B, C, and D) and of hydroxyapatite composites resulting from ice templating (E and F), revealing the similarities between the two structures. Scale bars are of length 5 (B), 0.5 (C), 0.3 (D), 300 (E), and 10 μm (F). Lower: compressive strength of porous HAP scaffolds (red solid triangles) as compared with data from the literature works cited in ref 53. The inset shows typical compression load−displacement curves for materials with 56% hydroxyapatite (HAP). Reprinted with permission from ref 54. Copyright 2006 American Association for the Advancement of Science.

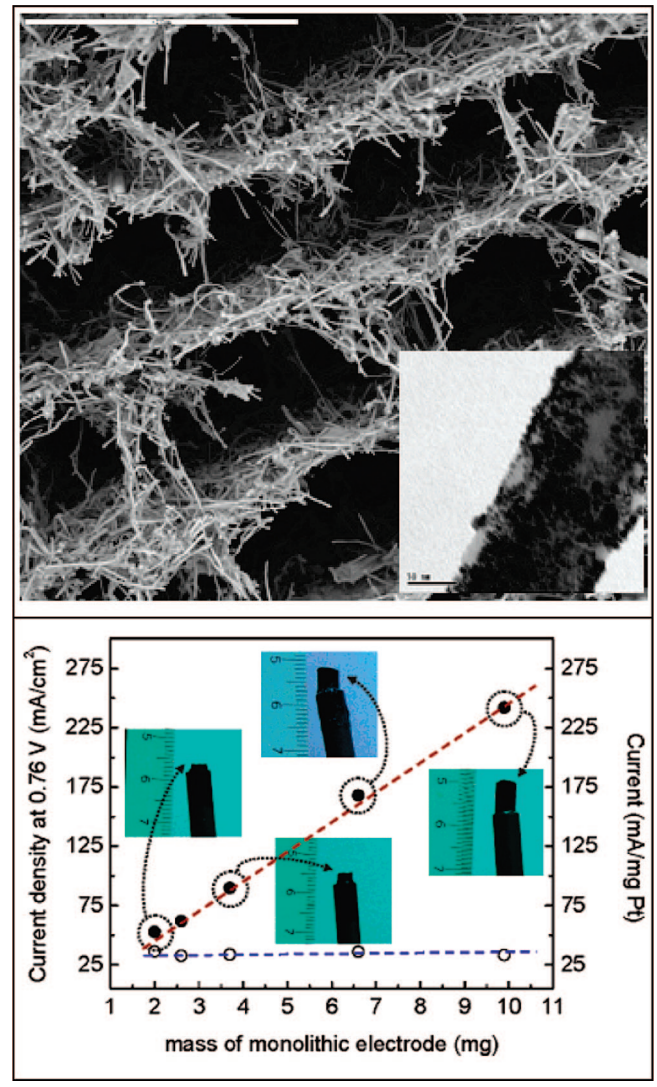

Figure 10. Upper: SEM micrograph of a cross-sectioned monolithic Pt/MWCNT 3D architecture (the bar is 20 μm in length). The inset shows a TEM micrograph of the MWCNT surface decorated with Pt nanoparticles (here the bar is 50 nm). Lower: plot of current density (solid symbols, left ordinate) and normalized current (open symbols, right ordinate) versus mass of Pt/MWCNT 3D monolith (abscissa). The data presented were obtained after scanning for 10 cycles (5 mV s^{-1} scan rate) to ensure a stable response. Reprinted with permission from ref 56. Copyright 2007 American Chemical Society.

the macrostructure. This may open a path toward a number of promising applications, mainly in drug delivery and catalysis. Eventually, ternary assemblies formed from colloidal silica and liposomes of two different compositions should be capable of preparation. In such systems, it might be possible individually to trigger the response of the different liposomes integrated within the assembly by subjecting it to, for example, two different temperatures.[46] One can envision the medical application of smart scaffolds for tissue engineering able to release growth factors (and thus promote tissue growth) and antibiotics from two such different liposomes, the former in a continuous mode and the latter only if the temperature rises above 39–40 °C as a consequence of an eventual infection resulting from or subsequent to surgery.

More recently, Cooper and co-workers have published a protocol for the ice-templated preparation of uniform spherical beads, produced via the colyophilization of α-chymotrypsin and different mixtures of polystyrene sodium sulfonate, PVA, dextran, Ludox HS30 silica nanoparticles, poly(ethylene glycol), and sodium dodecyl sulfate.[47] The use of simple PVA solutions, and of PVA in combination with nanoparticles, had been previously reported by the same authors.[48] It was demonstrated how ice templating can be used to generate a diverse array of complex structures such as polymer−inorganic nanocomposites, aligned gold microwires and microwire networks, porous composite microfibers, and biaxially aligned composite networks (Figure 7). In the case of the chymotrypsin spheres, the hierarchical structure of the composites (with up to five levels of spatial organization) provides particular functional and structural properties. Thus, the composites were assayed for catalytic activity by monitoring a nonaqueous transesterification reaction, while their mechanical strengths were measured using a compression assay. Initial screening identified a set of six support materials that contributed favorably to either

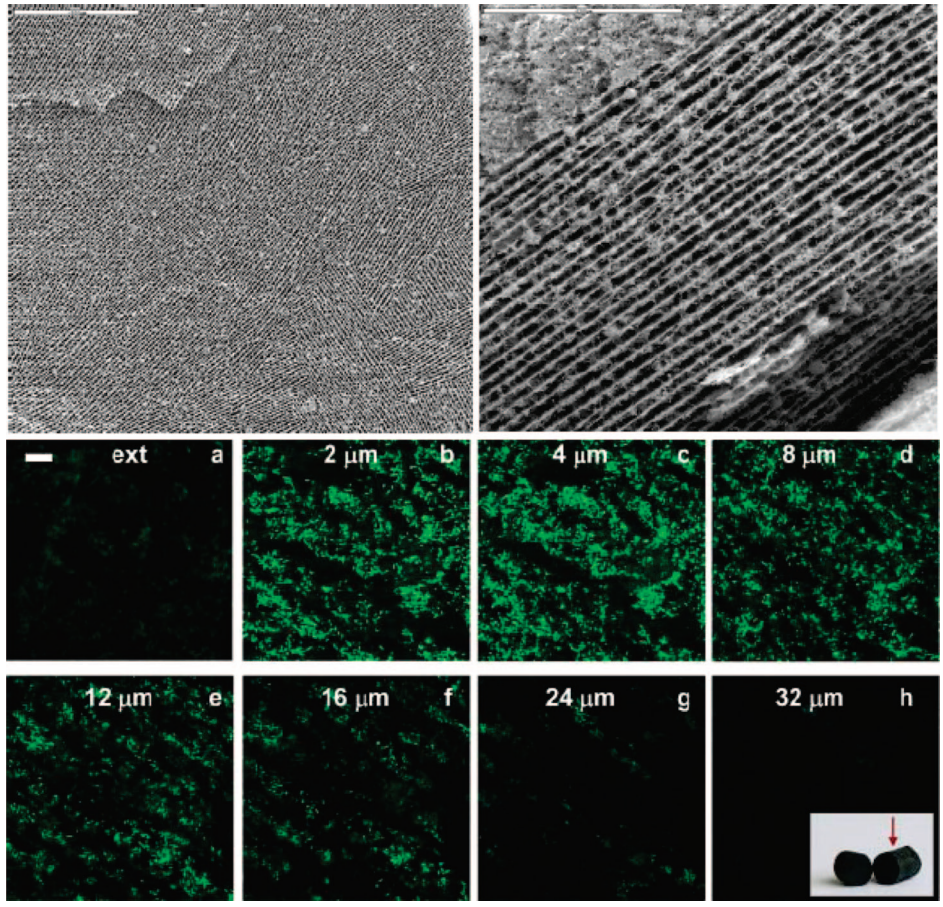

Figure 11. Upper half: SEM micrographs of a well-structured MWCNT/CHI 3D architecture over large extended areas (up to 2 mm) both in cross section (left; the bar is 500 μm long) and in longitudinal section (right; bar 200 μm) of the monolith. The unstructured zones at the upper-left and lower-right corners of the right-hand micrograph correspond to the external surface of the monolith. Lower half: confocal fluorescence microscopic images of the MWCNT/CHI 3D architecture after soaking for 24 h in a suspension of bacteria in culture medium. The depth of focus was set for (a) the external surface and (b) 2, (c) 4, (d) 8, (e) 12, (f) 16, (g) 24, and (h) 32 μm below it. The bar is 20 μm. Note that the fluorescent bacteria reproduce the morphology of the scaffold (eventually, the longitudinal section given the view angle used for confocal fluorescent images, see inset) due to bacterial adhesion to the MWCNT scaffold. Reprinted with permission from ref 66. Copyright 2007 Royal Society of Chemistry.

the enzyme activity or the mechanical strength of the composite. A design-of-experiments methodology was employed to screen 80 combinations of these six "base" materials. A model representing this formulation space was constructed which could be used to predict both the catalytic activity and mechanical strength with reasonable accuracy for any combination of the six base component materials. The model was used to predict optimized materials with an enzyme activity that was 50 times greater than that of the free enzyme and to set a minimum acceptable level of mechanical stability for these composites, one which would ultimately allows reusability for at least 10 reaction cycles. Somewhat disappointingly, it was found that the composites which produced the strongest beads were also associated with the lowest catalytic activity.[47]

The immobilization of whole organisms (even the simplest ones, such as bacteria) within the macroporous structure of a cryogel obviously implies further difficulty.[49] Interest in the immobilization of microbial cells in membranes and bioreactors resides in the achievement of enhanced catalytic activity and stability (as a result of enhanced protection of the microorganism from mechanical degradation and deactivation), which ultimately generates an overall intensification of the biochemical reactions of concern.[50] In particular, bacteria and other microbial cells can be used for bioremediation and biocatalysis, offering the possibility of decontaminating polluted environmental media and of implementing environment-friendly synthetic chemoenzymatically catalyzed processes.[51] The study of bacterial growth and proliferation in three-dimensional (3D) scaffolds is typically achieved by soaking the scaffold in a cell suspension. However, cell proliferation throughout the entire scaffold structure is impeded using this procedure, and colonization is limited to just a few layers at the periphery of the scaffold.[52] It should be noted that scaffold colonization occurs initially at the periphery and that nutrients and oxygen tend to be consumed by such outer bacteria before they can diffuse to the inner reaches of the scaffold. This problem would be overcome to a large extent if cells could be grown from the inner to the outer parts of the scaffold. As described above for liposomes, the application of the ISISA process to bacteria suspended in an aqueous PVA solution could provide a PVA scaffold with immobilized bacteria throughout its 3D structure. However, in the case of liposomes, preservation of their membrane structure occurs only in those cases in which the thickness of the walls that support the scaffold macrostructure is able fully to embed such membranes.[43,53] Bacteria are typically much larger than

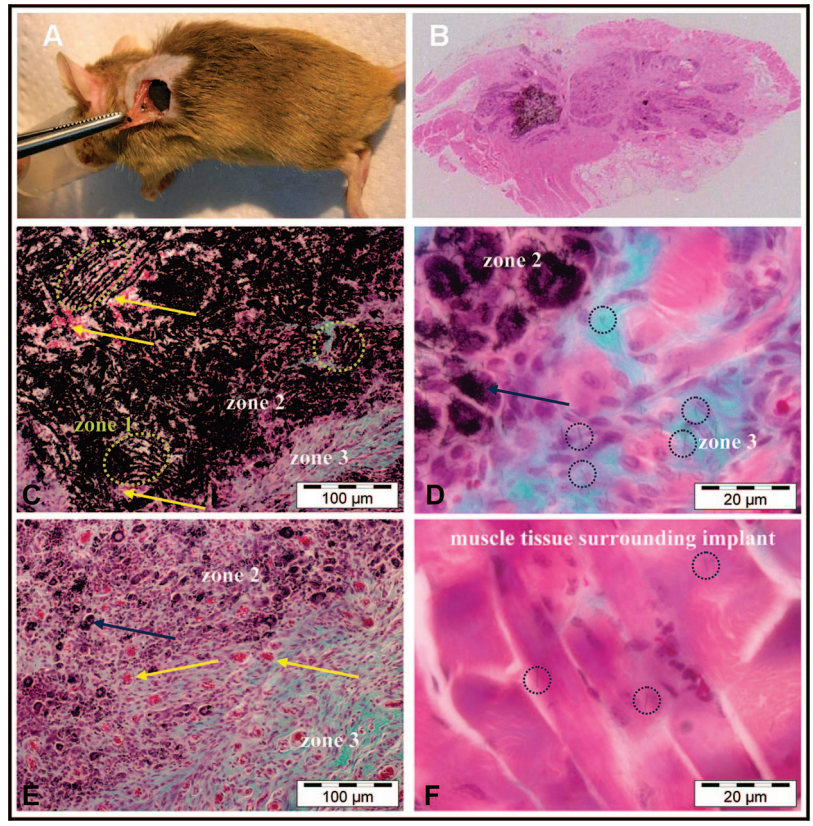

Figure 12. Picture A shows a surgical implantation of MWCNT/CHI scaffolds containing adsorbed rhBMP2 into a mouse subcutaneous muscular pocket. Optical micrograph B shows regenerated bone tissue and the small fraction of MWCNT/CHI scaffold remaining 3 weeks after scaffold implantation. Optical micrographs C−F show details of the three main distinguishable zones observed in micrograph B: zone 1 where the MWCNT/CHI scaffold structure remains basically intact (marked by green circles), zone 2 where nondifferentiated fibroblasts (purple cells) are colonizing the partially disassembled structure of the MWCNT/CHI scaffold (the positions of representative clusters of MWCNT/CHI aggregates are indicated by blue arrows), and zone 3 where the MWCNT/CHI scaffold is fully disassembled and individual MWCNT/CHI (the locations of some representative MWCNT/CHI are indicated by blue circles) are dispersed within the regenerated bone tissue (collagen expressing cells are colored blue-green). Note the abundance of blood vessels (containing erythrocytes, of which some representative examples are indicated by yellow arrows) in zone 2. Optical micrograph F shows a few individual MWCNT/CHI (also located within blue circles) dispersed within muscle tissue (colored pink) surrounding the implant. Reprinted with permission from ref 69. Copyright 2007 Elsevier.

scaffold wall thicknesses, so that bacteria are damaged upon simple ice-templating immobilization. Thus, our group has entrapped bacteria within beads composed of a natural calcium alginate polymer that contains glucose for further cryoprotection (Figure 8). A close inspection of the confocal fluorescence micrograph of this preparation shown in Figure 8 reveals high levels of bacteria comparable to those observed when the bacteria were immobilized by simple soaking of a preformed scaffold, in spite of the fact that the bacteria were not submitted to any cryogenic process.

3.2. Biomaterials and Biocomposites. In all of the above-mentioned ice-templated processes, freezing was performed either on hydrogels of either organic, inorganic or hybrid nature, or on ceramic slurries, the last only of inorganic nature. Tomsia and co-workers have demonstrated that the process also works for hybrid ceramic slurries.[54] There, the water suspension was frozen between two cold copper fingers whose temperature was regulated to control the speed of the solidification front. The presence of organics helps in the assembly of inorganic compounds, resulting in ultra-lightweight scaffolds with remarkable mechanical properties and whose macrostructure mimics that of nacre (Figure 9). In particular, these workers have prepared scaffolds comprising a major component of ceramic nature (e.g., hydroxyapatite), together with a more minor one (e.g., a polymer resin) playing the role of filler/binder. Thanks to their hybrid nature and morphology, the resulting biomaterials exhibited stiffness (10 GPa), strength (150 MPa), and work of fracture (220 J/m^2),[54] all of which match those of compact bone for an equivalent mineral/organic content (around 60/40 vol %).[55] Figure 9 shows the remarkable improvement achieved with these samples as compared with what had previously been reported for differently prepared materials of similar compositions.

With a similar approach, our group has recently applied the ISISA process to a water suspension of multiwall carbon nanotubes (MWCNT) and chitosan (CHI)[56] to favor MWCNT dispersion and ensure homogeneity of the suspension.[57] The resulting 3D architectures are highly porous (specific gravity ca. $\sim 10^{-2}$) and extremely conductive (up to 2.5 S/cm, depending on the MWCNT content) thanks to MWCNT interconnections in the macrostructure (Figure 10). The achievement of CNT-based 3D architectures is of special relevance since, except for a few recent cases,[58] most of the arrays prepared to date with controlled areas and nanotube lengths were two-dimensional (2D).[59−62] In particular, MWCNT/Pt-NP 3D architectures, prepared from MWCNT which are surface decorated with Pt nanoparticles (Pt-NP) previous to its assembly into the 3D architecture, have allowed a remarkable improvement in the catalysis of

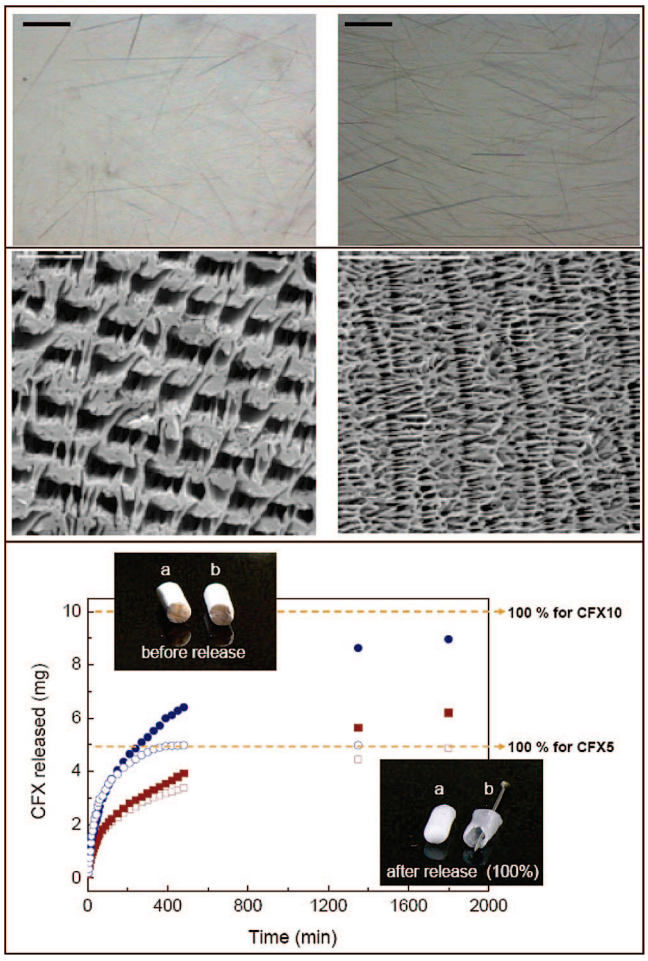

Figure 13. Upper half: Optical microscope images of CFX needles dispersed in an aqueous PVA solution at (upper left) 5 mg/mL and (upper right) 10 mg/mL (bars are 50 μm in length); SEM micrographs of PVA scaffolds (average molecular weight 72 000) prepared at freezing rates of (lower left) 0.7 and (lower right) 9.1 mm/min (bars are 20 μm). Lower half: Kinetics of CFX release from scaffolds prepared at freezing rates of 0.7 (red squares) and 9.1 mm/min (blue circles). Experiments were conducted on scaffolds containing 5 (open symbols) and 10 mg (solid symbols) of CFX, respectively. Dashed orange lines indicate 100% CFX release. Photographs of monolithic PVA2−CFX5 scaffolds prepared at freezing rates of (a) 0.7 and (b) 9.1 mm/min are also shown. Before release: lyophilized gels. After release: wet gels. In the latter case, erosion can be seen in the PVA2−CFX5 scaffold prepared at a freezing rate of 9.1 mm/min. Reprinted with permission from ref 75. Copyright 2007 Wiley-VCH.

methanol oxidation. It is noted that current densities of up to 242 mA/cm^2 are obtained thanks to the facile molecular transport of fuels and products throughout the microchanneled structure of the monolith. It is noteworthy that the mass activity (Figure 10, open circles, blue dashed line, right ordinate in mA/mg of Pt) remains constant, which property reflects the equivalent accessibility of every single Pt nanoparticle in the whole MWCNT 3D architecture.

The macrostructural features of MWCNT/Pt-NP 3D architectures with microchannels of ca. 20 μm diameter render them potentially useful as anodes in microbial fuel cells (MFC). Recent works have demonstrated the feasibility of using a variety of bacteria and other microorganisms to produce energy.[63] For MFC, efficient electron transfer between the microorganism and the anode (e.g., microorganisms forming a biofilm on graphite fibers) seems to play a major role in the performance of the fuel cell.[64] Thus, the MWCNT 3D architectures described above might simultaneously offer a suitable support through which bacteria can grow and proliferate and a large electrode surface area for electron transfer.[65] For this purpose, our group has immobilized bacteria within MWCNT scaffolds,[66] following a similar approach to that described above for PVA scaffolds. Preliminary results have demonstrated the excellent biocompatibility of MWCNT for immobilization of *E. coli* (Figure 11), albeit that further cryoprotection seems to be required during the ISISA process for enhanced bacteria viability.

The efficient growth and proliferation of *E. coli* throughout the whole scaffold structure indicates that MWCNT scaffolds may also form suitable substrates for other types of cell cultures. However, some controversy exists in regard to the biocompatible character of SWCNT and MWCNT with eukaryotic cells. Thus, some in vitro studies have reported that CNT are cytotoxic[67] while others show CNT to be excellent substrates for cellular growth.[68] In the particular case of ISISA-prepared MWCNT scaffolds, our group has recently reported ectopic bone formation in muscle tissue by implantation of MWCNT scaffolds containing rhBMP-2 (a potent osseo-inductor protein that promotes the differentiation of differentiated cells into an osteoblastic lineage) adsorbed onto the macrostructure (Figure 12).[69] The excellent MWCNT biocompatibility observed in our case was ascribed to the purification process used for MWCNT, which eliminated metal traces and amorphous carbon,[70] typical byproducts resulting from MWCNT preparation procedures, prior to formation of the scaffold.[71] It is noted that metals[72] and amorphous carbon[73] are reported to be the major factors responsible for MWCNT cytotoxicity. Additionally, the chitosan used for MWCNT dispersion in water at least partially covers the surface of the MWCNT forming the scaffold after ISISA process, and this is also well-known to be of help in further improving biocompatibility.[74]

However, the use of suspensions for preparation of ice-templated materials is not restricted only to those which are ceramic or CNT based. Thus, our group has extended this approach to organic crystalline needles (e.g., ciprofloxacin, CFX) suspended in an aqueous solution of PVA (Figure 13).[75] CFX is a synthetic fluoroquinolone antimicrobial agent whose primary mechanism of action against bacteria (both Gram-positive and Gram-negative) involves inhibition of topoisomerase IV and DNA gyrase.[76] The CFX crystalline needles were prepared in situ by incorporation of doubly lyophilized CFX into a warm (90 °C) solution of PVA. Cooling down to room temperature promotes CFX crystallization in the form of needles homogenously suspended in the PVA solution. ISISA processing of this suspension results in the formation of PVA scaffolds with crystalline CFX needles homogeneously entrapped within the PVA fences that maintain the microchannel structure. The resulting PVA−CFX scaffolds were used for controlled delivery and release of the drug, special attention being paid to the influence of the scaffold morphology (mainly tailored by the use of different freezing rates, see Figure 13) on the kinetics of release of the drug. The extremely different morphologies of the scaffolds achieved (one with narrow channels separated by thin walls of matter, another with wide channels

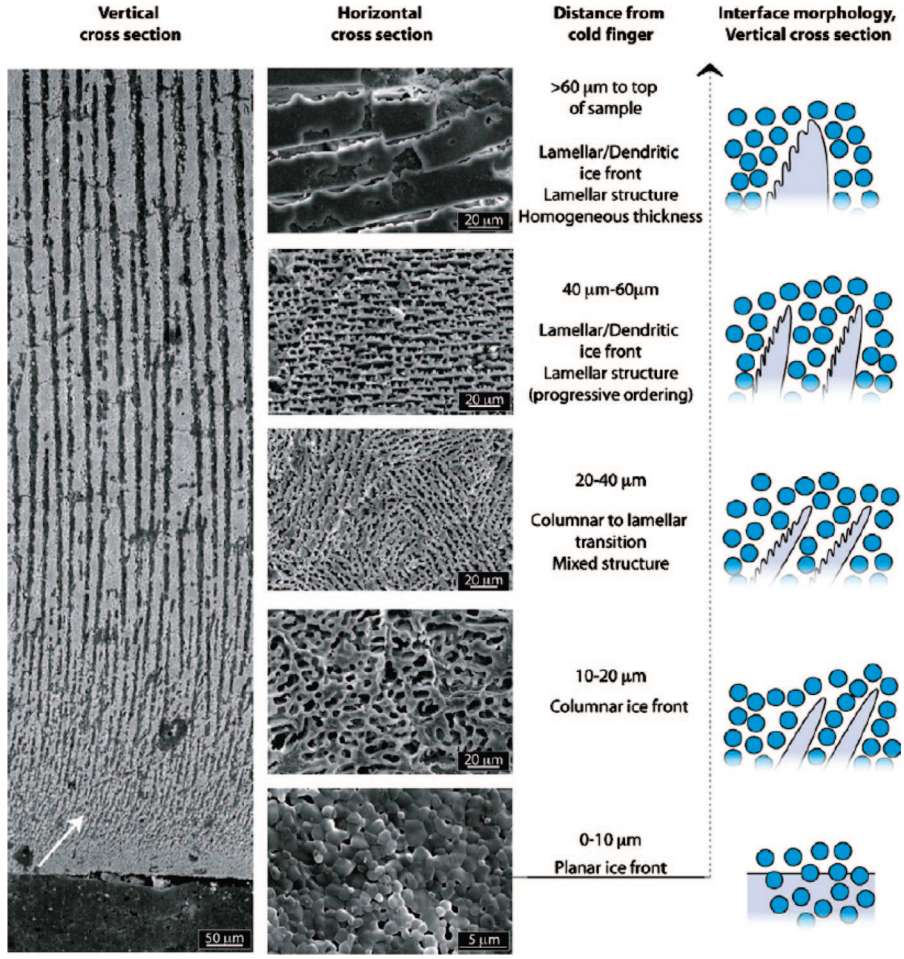

Figure 14. SEM micrographs of the evolution of the ice-front morphology and final microstructure. Homogeneous layer thickness is attained at about 200–250 mm above the immersion level—the layer thickens progressively with the separation from the immersion level and then becomes constant. Tilting of the lamellae in the first frozen zone can be observed near the immersion level, at the bottom of the vertical-section micrograph (white arrow). The horizontal cross section (parallel to the ice front) micrographs reveal the corresponding evolution of the porous structure and hence the interface morphology (depicted diagrammatically on the right). Reprinted with permission from ref 38d. Copyright 2007 Elsevier.

separated by thick walls of matter) determine different rates of controlled release. Thus, release from the scaffold characterized by narrow channels is mainly based on scaffold erosion and allows fast release kinetics (ca. 50% in just 45 min), while release from the scaffold characterized by wide channels is based on scaffold hydration, swelling, and dissolution of the entrapped drug and can be extended for longer periods of time (complete release needing more than 30 h) (Figure 13). The interest in introducing CFX as crystalline needles resides in the possibility of loading the PVA scaffold with different drug concentrations without altering the scaffold morphology (which ultimately determines the kinetic release). Thus, we can release the proper drug dose at a higher than minimum inhibitory concentration, but without any risk of toxic overdoses.[16,77] In vitro experiments have also demonstrated the ability of PVA−CFX to inhibit the growth of *E. coli* in different culture media.[75]

Morphology Control in Ice-Templating Processes

On the basis of the examples described above, it is easy to appreciate the tremendous versatility of ice-templating processes for the preparation of scaffolds with a variety of compositions (inorganic, organic, hybrid, biohybrid, composites, and biocomposites) and excellent control of structural features, both at the micro- and nanoscale. The simplicity of the process can also be readily appreciated: the final microstructure is, ultimately, always a replica of the ice, no matter how the freezing might be achieved by different thermal treatments, e.g., freezing of the aqueous medium by immersion in cryogenic liquids of different nature or by the application of some other kind of freezing device.

The main process control variables available to tailor the final morphology were first studied by Tamon and co-workers[38a,b] and more recently overviewed extensively by Tomsia and co-workers.[38c,d] One of the most interesting observations made by the latter authors concerns the structural heterogeneity of the sample in the freezing direction (Figure 14). Three distinct zones can be clearly distinguished in the samples, each characterized by a particular pore shape and dimension. In zone 1, the closest to the initial coldfinger, no porosity at all is observed, and the material is dense. In the second zone, the material is characterized by a cellular morphology. Finally, in the upper zone (zone 3), the ceramic is lamellar (with interlamellar

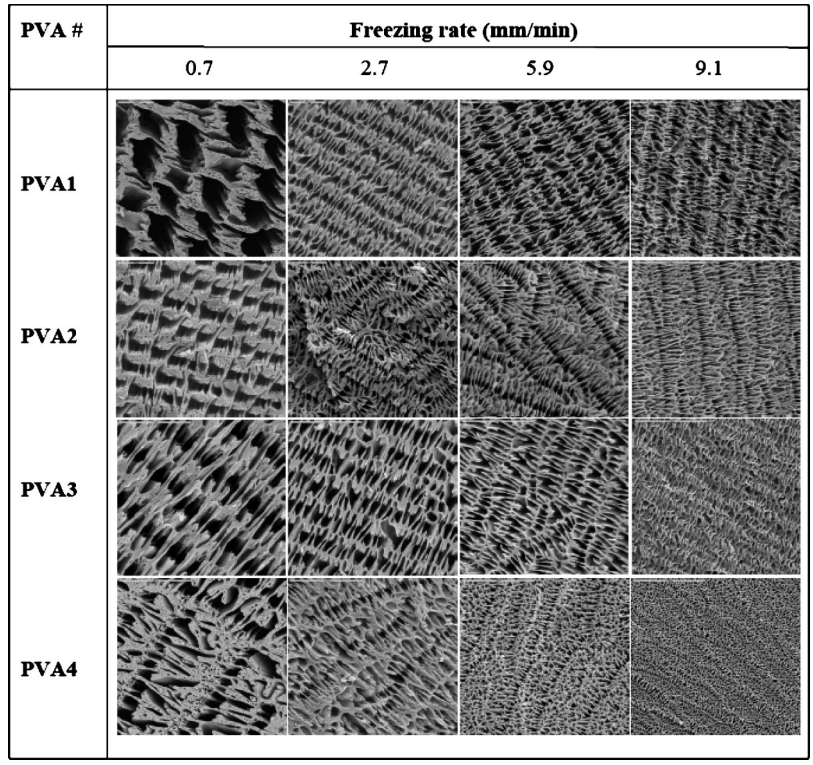

Figure 15. SEM micrographs of cross-sectioned (perpendicular to the direction of freezing) monolithic PVA scaffolds. These tailored morphologies were obtained by using PVA with different average molecular weights (13 000–23 000 for PVA1; 72 000 for PVA2; 89 000–98 000 for PVA3; 132 000 for PVA4) and by processing the PVA solution at different freezing rates. The bar is 20 μm in length in every picture. Note that, in some cases, the actual magnification (indicated by the length of the bar scale) is varied for better visualization of the scaffold macrostructure. The PVA content of all of the samples was 7.8 wt %. Reprinted with permission from ref 75. Copyright 2007 Wiley-VCH.

separation defined by λ, see Figure 1), with long parallel pores aligned in the direction of movement of the ice front. When the probe is immersed in liquid nitrogen (i.e., at −196 °C), the water supercools, and amorphous rather than crystalline ice is formed. The formation of amorphous ice does not occur when pure water is frozen at this temperature (even though it is well below the glass transition temperature of water, $T_g \sim -137$ °C), since T_g is not an equilibrium transition temperature and hence, being only quasi-thermodynamic, may vary with experimental conditions.[78] Freezing rates of ca. 10^6 °C/s are required if one desires to obtain amorphous ice from pure water.[79] However, ice crystallization also depends on the presence of impurities in the water, being fully inhibited for pseudoconcentrated solutions: threshold values of concentration bringing about this inhibition vary widely and depend on the nature of the solute. Thus, when a water solution/suspension or gel is just partially immersed into liquid nitrogen, the presence of solutes determines the formation of amorphous ice in the immersed portion, so that neither matter segregation nor formation of any porous structure occurs (zone 1). Meanwhile, an ice front running along the nonimmersed portion of the probe can be visualized. The temperature at the ice front is obviously higher than that of liquid nitrogen because of differential diffusion of heat coming in from the environment surrounding the probe (air and liquid nitrogen, respectively). The further the ice front moves away from the liquid nitrogen immersion level, the more its temperature increases. Eventually, it is not low enough for supercooling to occur, and so crystalline rather than amorphous ice is formed. As pointed out above, the formation of crystalline ice determines matter of segregation and results in the formation of porous structures after freeze-drying. The pore size depends on the distance from the liquid nitrogen immersion level (i.e., small in zone 2, where temperatures are still close to that of liquid nitrogen, but large at zone 3, where temperatures are higher) so that the resulting scaffold exhibits a longitudinal pore size heterogeneity. Homogeneous tailoring of the microchanneled structure is realizable by not just partial, but continuous, immersion (at a constant rate) into liquid nitrogen. Under these circumstances, the ice front is forced closer to, and eventually (at high freezing rates during rapid immersion) coincides with, the liquid nitrogen immersion level. Thus, the microchanneled structure formed at zone 3 is characterized by narrower channels (the closer to the liquid nitrogen immersion level, the narrower the channels) as a consequence of the smaller size of the ice crystals formed (Figure 15).[75]

The formation of small or large ice crystals upon freezing is also related to both the solute concentration in the solution/suspension or gel and the solute size. The ability for ice-crystal growth in the presence of a given solute depends on the adsorption/desorption balance of the particular solute at the ice-crystal surface. Irreversible adsorption would completely abrogate ice-crystal growth, while complete desorption would allow free crystal growth. In practice, adsorption and desorption at the ice surface are in dynamic equilibrium. For a particular solute, the effectiveness in inhibiting the growth of ice crystals simply depends on the extent of the surface area of ice that is covered by such a solute. Thus,

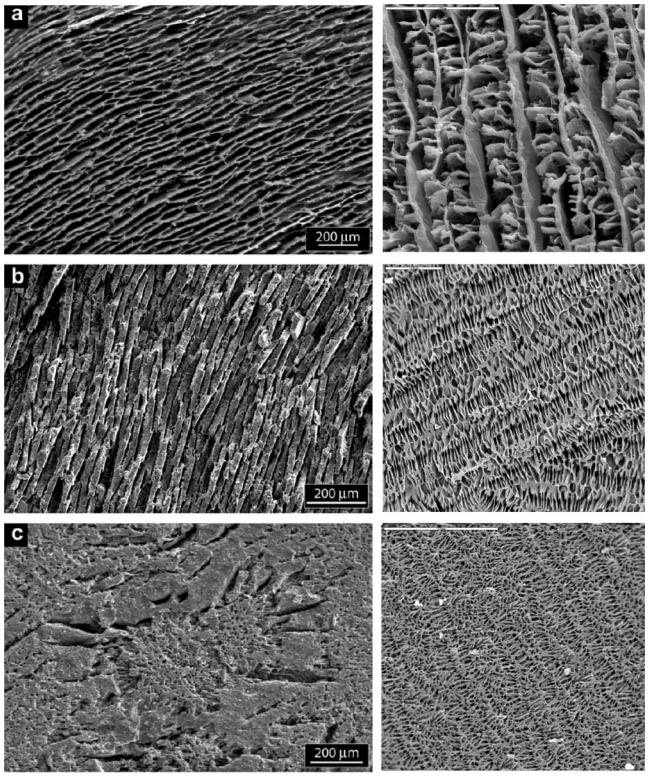

Figure 16. SEM micrographs of cross-sectioned (perpendicular to the direction of freezing) monolithic ceramic (left column) and PVA (right column) scaffolds for different solute contents. From top to bottom: 30, 60, and 76 wt % in left column (bars are 200 μm in length) and 2.5, 7.8, and 10 wt % in right column (bars are 20 μm). From refs 38d and 75. Copyright 2007 Elsevier and Wiley-VCH.

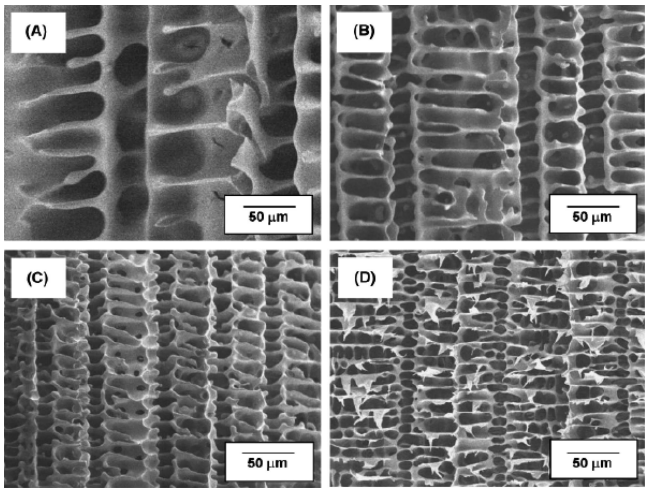

Figure 17. SEM micrographs of porous polycarbosilane cryogels prepared at freezing temperatures of (A) 20, (B) 0, (C) −20, and (D) −40 °C, using a PCS concentration of 10 wt %. Reprinted with permission from ref 82c. Copyright 2007 American Chemical Society.

large solutes and/or high solute concentrations yield small crystals, while small solutes and/or low solute concentrations yield large ones (Figures 15 and 16). As regards solute size, Tomsia and co-workers have found an empirical dependence of λ on the speed of the ice front in the direction parallel to the temperature gradient ($\lambda \sim v^{-n}$), n being related to the particle size of the suspended solute so that the larger the particle size, the narrower the interlamellar separation.[38d] Under the same principle (i.e., inhibition of ice-crystal growth

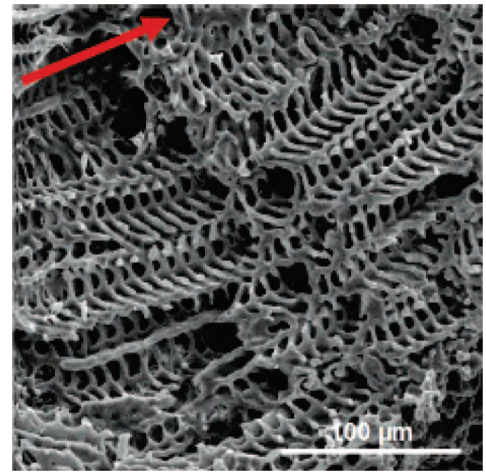

Figure 18. SEM micrographs of aligned porous BGAL produced by directional freezing of a liquid CO_2 solution. The red arrow represents the approximate direction of freezing. Reprinted with permission from ref 83. Copyright 2005 American Chemical Society.

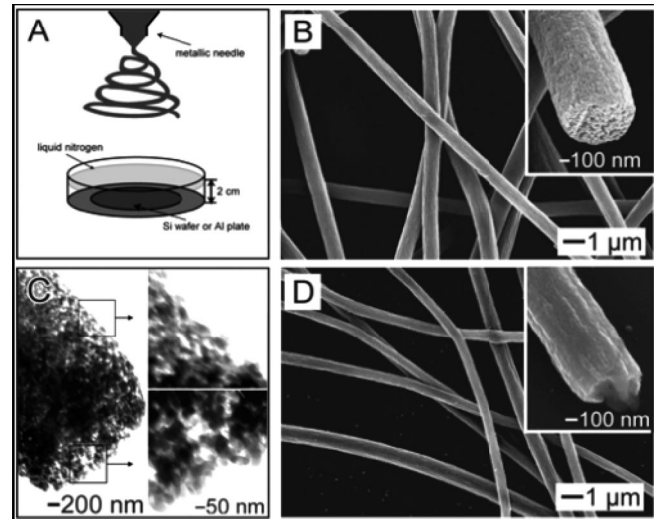

Figure 19. (A) Electrospinning setup with the modified collector used to produce porous polystyrene fibers. A polystyrene dish was used to hold the liquid nitrogen bath, while the rest of the setup was similar to those used in previous studies. (B) SEM images of porous polystyrene fibers prepared by the electrospinning of solutions of polystyrene in dimethylformamide into liquid nitrogen, followed by drying under vacuum. The insert is an SEM micrograph of the broken end of a fiber at a higher magnification, showing that the fiber was porous throughout. (C) TEM of the porous polystyrene fibers shown in (B), with inserts at higher magnification. (D) Polystyrene fibers electrospinning into liquid nitrogen in the same way, but then reheated rapidly to room temperature in air: note the lack of porosity and lower surface roughness of these fibers. Reprinted with permission from ref 84a. Copyright 2006 American Chemical Society.

determined by the extent to which the solute covers the ice surface), solute concentration also plays a role in tailoring the final morphology of the microchanneled structure. Eventually, very high solute concentrations would fully inhibit ice-crystal formation and thus the formation of any microchanneled structures at all. On the other side of the coin, though, very low concentrations may yield mechanically weak microchanneled structures as consequence of the resulting small amount of matter supporting the whole structure.

Another interesting microstructural feature is the formation of translamellar bridges when the solute concentration

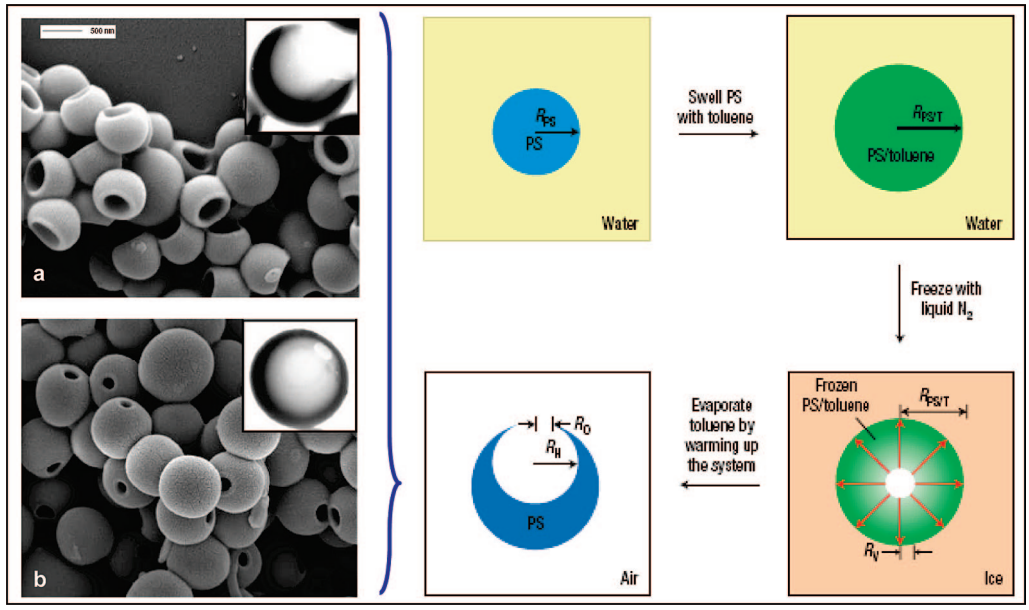

Figure 20. Right: schematic illustration of the three major steps involved in the formation of hollow polystyrene particles with holes in their surfaces. Left: SEM micrographs of hollow polystyrene particles with holes in their surfaces, derived from solid polystyrene beads. The beads in (a) and (b) were swollen by toluene and styrene, respectively, frozen in liquid nitrogen, and the solvent then evaporated off under vacuum for 1 day. Reprinted with permission from ref 84b. Copyright 2005 Nature Publishing Group.

reaches certain values. In materials of ceramic nature, such translamellar bridges are rather fine and often display somewhat tortuous and irregular morphologies, while in hybrid materials (e.g., MWCNT/CHI-based ones, Figure 10), the regularity of the pattern formed by such bridges is remarkable. The mechanism governing bridge formation is unknown; that is, while for ceramic materials it seems to occur with highly concentrated slurries and slow freezing rates, for hybrid materials it occurs at intermediate values of both concentration and freezing rate. Further work is needed to clarify the origin and conditions of formation of these interesting bridges which break the typical anisotropy of unidirectionally frozen cryogels and, hence, should contribute to an overall improvement in the stability and mechanical properties of the whole macrostructure.

Conclusions

In summary, we hope that this review might encourage further uses of ice-templating processes for preparation of new materials with highly sophisticated structures, even while emphasizing that ice-templating has indeed been in use for a long time in the preparation of a variety of structured materials, mostly scaffolds of polymeric nature for tissue engineering purposes. We apologize to the authors of those excellent works that due to the large activity in such an area and restrictions on the size of this review, we have had to omit. Thus, we do not claim that this review includes all—or even most—of the published work but rather comprises an exposition of some of the most recent applications of ice-templating, mainly in its application to aqueous solutions/suspensions and hydrogels of diverse nature and highlighting its success in controlling the morphology of the product.[38] This success in the control of product morphology is undoubtedly the reason that ice-templating processes are lately attracting more and more attention. This review has emphasized and exemplified the way in which the aqueous nature of this process allows the achievement of hierarchical materials with a rich diversity of different levels of spatial organization, ultimately providing functionality to the resulting materials. This combination of hierarchy and functionality opens up the possibility of application of these "smart" materials to a variety of novel applications in such fields as biotechnology (e.g., biosensors and biocatalytic systems for organic synthesis and fuel cell technologies, among those reviewed in this work) and biomedicine. Furthermore, even in the latter case, where cryogels have for some time been widely used for tissue engineering and drug delivery purposes, control of the morphology and the possibility of extending the composition of the scaffolds to hybrids and biohybrids have already allowed, and will increasingly in the future allow, the preparation of scaffolds exhibiting enhanced functional (in terms of both biocompatibility and biodegradability)[80] and mechanical[38c,54] performance. Gabriel García Márquez wrote in *One Hundred Years of Solitude* how Aureliano Buendia was fascinated when he discover ice ("Many years later, as he faced the firing squad, Colonel Aureliano Buendía was to remember that distant afternoon when his father took him to discover ice."). Apparently, there is still much to discover (and to be fascinated) about ice, in particular, how it behaves in presence to different colloidal additives and how we can take advantage of such a behavior to create novel structures/materials.

Acknowledgment. The authors thank the MEC, CSIC, and Comunidad de Madrid for financial support (MAT2006-02394, 200660F01, 200760I009, and S-0505/PPQ-0316 Projects). TPA Inc. is also acknowledged for valuable support. M.C.G. acknowledges the CSIC for an I3P research contract. The contributions of Prof. Robert E. Dale, Prof. Fredric M. Menger, Prof. Fernando Rojo, Dr. Ricardo Jimenez, Dr. Manuel Amarilla, Prof. Fernando Catalina, Dr. Matias Jobbagy, and the Group of

Bioinspired Materials to the development of this work are gratefully acknowledged.

Appendix. Freezing of Nonaqueous Solutions: Other Well-Ordered Macrostructures

This review has been focused on materials resulting from ice templating because of our own particular interest in aqueous processes for preparation of hierarchically organized materials of interest in biotechnology and biomedicine. However, it must also be acknowledged that the preparation of templated materials by freezing procedures with good control of the morphology is not restricted to aqueous solutions. Highly interesting materials in terms of both composition and structure have also recently been prepared by freezing nonaqueous solutions. For instance, Halloran and co-workers first,[81] and Kim and co-workers more recently,[82] have reported the achievement of highly porous ceramics with three-dimensionally interconnected pore channels of up to 100 μm diameter and thus of great interest for applications in bone tissue engineering, by freezing camphene slurries (e.g., alumina- or hydroxyapatite-based) and solutions (e.g., polycarbosilane), which thereafter are freeze-dried and calcined at high temperatures (Figure 17). Cooper and co-workers have also recently shown how cryogenic processes can result in materials with very interesting morphologies when CO_2 (rather than water) is used as solvent.[83] In that particular case, 1,2,3,4,6-pentaacetyl-β-D-galactose (BGAL, a sugar acetate) was dissolved (with the help of ultrasonication) in liquid CO_2 and lowered vertically into liquid nitrogen (at a rate of 3.2 mm/min) until the column was completely submerged, at which point the sample was no longer under excess pressure since all of the CO_2 was frozen into the solid state. The column was then transferred into a beaker containing dry ice, and a venting valve was opened to allow gaseous CO_2 to escape from the column as it sublimed from the sample during slow warming. The BGAL sample (which was supplied as a powder) was then recovered directly from the tube as a continuous monolith with the macroporous structure shown in Figure 18. Finally, Xia and co-workers have also used a similar cryogenic process for the achievement of highly porous polymer fibers and hollow polymer particles with holes of controllable size in their surfaces. The former were obtained by electrospinning a dimethylformamide solution of a given polymer, e.g., polystyrene, poly(acrylonitrile), or poly(vinylidene fluoride), into a liquid nitrogen bath (Figure 19). The latter were formed by freezing swollen polystyrene beads suspended in a water/toluene solution (Figure 20), and in both cases, freeze-drying was used for solvent removal.[84]

Note Added after ASAP Publication. This paper published ASAP January 4, 2008 with an error in the Introduction section; the corrected version published ASAP January 11, 2008.

References

(1) Ozin, G. A.; Arsenault, A. C. *Nanochemistry: A Chemical Approach to Nanomaterials*; RSC Publishing: Cambridge, 2005.

(2) (a) Soler-Illia, G. J. A. A.; Sanchez, C.; Lebeau, B.; Patarin, J. *Chem. Rev.* **2002**, *102*, 4093. (b) Sanchez, C.; Arrivart, H.; Giraud-Guille, M. M. *Nat. Mater.* **2005**, *4*, 277. (c) Burda, C.; Chen, X.; Narayanan, R.; El-Sayed, M. A. *Chem. Rev.* **2005**, *105*, 1025.

(3) (a) Rhodes, K. H.; Davis, S. A.; Caruso, F.; Zhang, B.; Mann, S. *Chem. Mater.* **2001**, *12*, 2832. (b) Wang, D.; Caruso, R. A.; Caruso, F. *Chem. Mater.* **2001**, *13*, 364. (c) Yu, A.; Liang, Z.; Caruso, F. *Chem. Mater.* **2005**, *17*, 171.

(4) (a) DiMarzio, E. A.; Guttman, C. M.; Hoffman, J. D. *Macromolecules* **1980**, *13*, 1194. (b) Discher, B. M.; Won, Y.-Y.; Ege, D. S.; Lee, J. C.-M.; Bates, F. S.; Discher, D. E.; Hammer, D. A. *Science* **1999**, *284*, 1143. (c) Discher, D. E.; Eisenberg, A. *Science* **2002**, *297*, 967.

(5) Kresge, C. T.; Leonowicz, M. E.; Roth, W. J.; Vartuli, J. C.; Beck, J. S. *Nature (London)* **1992**, *359*, 710.

(6) (a) Carn, F.; Colin, A.; Achard, M.-F.; Deleuze, H.; Backov, R. *Adv. Mater.* **2004**, *16*, 140. (b) Grosso, D.; Cagnol, F.; Soler-Illia, G. J. A. A.; Crepaldi, E. L.; Amenitsch, H.; Brunet-Bruneau, A.; Bourgeois, A.; Sanchez, C. *Adv. Funct. Mater.* **2004**, *14*, 309. (c) Zhao, D.; Feng, J.; Huo, Q.; Melosh, N.; Fredrickson, G. H.; Chmelka, B. F.; Stucky, G. D. *Science* **1998**, *279*, 548. (d) Yang, P.; Zhao, D.; Margolese, D. I.; Chmelka, B. F.; Stucky, G. D. *Nature (London)* **1998**, *396*, 152. (e) Förster, S.; Antonietti, M. *Adv. Mater.* **1998**, *10*, 195. (f) Schüth, F. *Angew. Chem., Int. Ed.* **2003**, *42*, 3604.

(7) Fireman-Shoresh, S.; Avnir, D.; Marx, S. *Chem. Mater.* **2003**, *15*, 3607.

(8) (a) Kishida, T.; Fujita, N.; Sada, K.; Shinkai, S. *J. Am. Chem. Soc.* **2005**, *127*, 7298. (b) Moreau, J. J. E.; Vellutini, L.; Man, M. W. C.; Bied, C. *J. Am. Chem. Soc.* **2001**, *123*, 1509.

(9) Shin, Y.; Wang, C.; Exarhos, G. J. *Adv. Mater.* **2005**, *17*, 74.

(10) Weatherspoon, M. R.; Allan, S. M.; Hunt, E.; Cai, Y.; Sandhage, K. H. *Chem. Commun.* **2005**, 651.

(11) Huang, J.; Kunitake, T. *J. Am. Chem. Soc.* **2003**, *125*, 11834.

(12) Yang, D.; Qi, L.; Ma, J. *Adv. Mater.* **2002**, *14*, 1543.

(13) Mayes, E. L.; Vollrath, F.; Mann, S. *Adv. Mater.* **1998**, *10*, 801.

(14) Cook, G.; Timms, P. L.; Göltner-Spickermann, C. *Angew. Chem., Int. Ed.* **2003**, *42*, 557.

(15) Hall, S. R.; Bolger, H.; Mann, S. *Chem. Commun.* **2003**, 2784.

(16) Ogasawara, W.; Shenton, W.; Davis, S. A.; Mann, S. *Chem. Mater.* **2000**, *12*, 2835.

(17) (a) van Bommel, K. J. C.; Friggeri, A.; Shinkai, S. *Angew. Chem.* **2002**, *42*, 980. (b) Davis, S. A.; Breulmann, M.; Rhodes, K. H.; Zhang, B.; Mann, S. *Chem. Mater.* **2001**, *13*, 3218–3226. (c) Caruso, R. A.; Antonietti, M. *Chem. Mater.* **2001**, *13*, 3272.

(18) (a) Caruso, R. A.; Antonietti, M. *Adv. Funct. Mater.* **2002**, *12*, 307. (b) Sen, T.; Tiddy, G. J. T.; Casci, J. L.; Anderson, M. W. *Angew. Chem., Int. Ed.* **2003**, *42*, 4649. (c) Zhou, Y.; Antonietti, M. *Adv. Mater.* **2003**, *15*, 1452. (d) Villaescusa, L. A.; Mihi, A.; Rodriguez, I.; Garcia-Bennett, A. E.; Miguez, H. *J. Phys. Chem. B* **2005**, *109*, 19643.

(19) Antonietti, M.; Kuang, D.; Smarsly, B.; Zhou, Y. *Angew. Chem., Int. Ed.* **2004**, *43*, 4988.

(20) (a) Bigi, A.; Boanini, E.; Walsh, D.; Mann, S. *Angew. Chem., Int. Ed.* **2002**, *41*, 2163–2166. (b) Cölfen, H.; Mann, S. *Angew. Chem., Int. Ed.* **2003**, *42*, 2350–2365. (c) Payne, G. F. *Curr. Opin. Chem. Biol.* **2007**, *11*, 214. (d) Yuan, Z.-Y.; Su, B.-L. *J. Mater. Chem.* **2006**, *16*, 663.

(21) (a) Mann, S. *Biomimetic Materials Chemistry*; VCH Publishers: New York, 1996. (b) Mann, S. *Biomineralization: Principles and Concepts in Bioinorganic Materials Chemistry*; Oxford Chemistry Masters: Oxford, UK, 2001. (c) Bensaude-Vincent, B.; Arribart, H.; Bouligand, Y.; Sanchez, C. *New J. Chem.* **2002**, *26*, 1.

(22) Water is the universal solvent for life, referred to by Nobel Laureate A. Szent-György as "the matrix of life".

(23) Pate, J. W.; Sawyer, P. N. *Am. J. Surg.* **1953**, *82*, 3.

(24) Ross, D. N. *Lancet* **1962**, *2*, 487.

(25) Chen, G.; Ushida, T.; Tateishi, T. *Biomaterials* **2001**, *22*, 2563.

(26) Hoa, M.-H.; Kuoa, P.-Y.; Hsieha, H.-J.; Hsienb, T.-Y.; Houc, L.-T.; Laid, J.-Y.; Wang, D.-M. *Biomaterials* **2004**, *25*, 129.

(27) Kang, H.-W.; Tabata, Y.; Ikada, Y. *Biomaterials* **1999**, *20*, 1339–1344.

(28) Hsieh, C.-Y.; Tsai, S.-P.; Wang, D.-M.; Chang, Y.-N.; Hsieh, H.-J. *Biomaterials* **2005**, *26*, 5617.

(29) Ho, M.-H.; Wang, D.-M.; Liu, C.-E.; Hsieh, C. H.; Tseng, H.-C.; Hsieh, H.-J. *Carbohydr. Polym.* **2007**, *67*, 124.

(30) Daamen, W. F.; Van Moerkerk, H. Th. B.; Hafmans, T.; Buttafoco, L.; Poot, A. A.; Veerkamp, J. H.; Van Kuppevelt, T. H. *Biomaterials* **2003**, *24*, 4001.

(31) Dagalakis, N.; Flink, J.; Stasikelis, P. *J. Biomed. Mater. Res.* **1980**, *14*, 511.

(32) Shalaby, W. S. W.; Peck, G. E.; Park, K. *J. Controlled Release* **1991**, *16*, 355.

(33) Mahler, W.; Bechtold, M. F. *Nature (London)* **1980**, *285*, 27.

(34) Landsberg, A.; Campbell, T. T. *J. Met.* **1965**, 856.

(35) Johnson, D. W., Jr.; Schnettler, F. J. *J. Am. Ceram. Soc.* **1970**, *53*, 440.

(36) Gallagher, P. K.; Schrey, F. *Thermochim. Acta* **1970**, *1*, 465.

(37) (a) Fukasawa, T.; Ando, M.; Ohji, T.; Kanzaki, S. *J. Am. Ceram. Soc.* **2001**, *84*, 230. (b) Sofie, S. W.; Dogan, F. *J. Am. Ceram. Soc.* **2001**, *84*, 1459.

(38) (a) Mukai, S. R.; Nishihara, H.; Tamon, H. *Chem. Commun.* **2004**, 874. (b) Nishihara, H.; Mukai, S. R.; Yamashita, D.; Tamon, H. *Chem. Mater.* **2005**, *17*, 683. (c) Deville, S.; Saiz, E.; Tomsia, A. P. *Biomaterials* **2006**, *27*, 5480. (d) Deville, S.; Saiz, E.; Tomsia, A. P. *Acta Mater.* **2007**, *55*, 1965.

(39) (a) Nishihara, H.; Mukai, S. R.; Tamon, H. *Carbon* **2004**, *42*, 889. (b) Tamon, H.; Ishizaka, H.; Yamamoto, T.; Suzuki, T. *Carbon* **2000**, *38*, 1099. (c) Mukai, S. R.; Nishihara, H.; Yoshida, T.; Taniguchi, K.; Tamon, H. *Carbon* **2005**, *43*, 1557. (d) Tamon, H.; Ishizaka, H.; Yamamoto, T.; Suzuki, T. *Carbon* **1999**, *37*, 2049.

(40) Nishihara, H.; Mukai, S. R.; Fujii, Y.; Tago, T.; Masuda, T.; Tamon, H. *J. Mater. Chem.* **2006**, *16*, 3231.

(41) Mukai, S. R.; Nishihara, H.; Shichi, S.; Tamon, H. *Chem. Mater.* **2004**, *16*, 4987.

(42) Gutierrez, M. C.; Jobbagy, M.; Rapun, N.; Ferrer, M. L.; del Monte, F. *Adv. Mater. (Weinheim, Ger.)* **2006**, *18*, 1137.

(43) Ferrer, M. L.; Esquembre, R.; Ortega, I.; Mateo, C. R.; del Monte, F. *Chem. Mater.* **2006**, *18*, 554.
(44) Toone, E. J.; Werth, M. J.; Jones, J. B. *J. Am. Chem. Soc.* **1990**, *112*, 4946.
(45) Chen, F.-E.; Chen, X.-X.; Dai, H.-F.; Kuang, Y.-Y.; Xie, B.; Zhao, J.-F. *Adv. Synth. Catal.* **2005**, *347*, 549.
(46) Chen, W.-H.; Regen, S. L. *J. Am. Chem. Soc.* **2005**, *127*, 6538.
(47) Long, J.; Hutcheon, G. A.; Cooper, A. I. *J. Comb. Chem.* **2007**, *9*, 399.
(48) Zhang, H.; Hussain, I.; Brust, M.; Butler, M. F.; Rannard, S. P.; Cooper, A. I. *Nat. Mater.* **2005**, *4*, 787.
(49) Gutierrez, M. C.; Garcia-Carvajal, Jobbagy, M.; Yuste, L.; Rojo, F.; Abrusci, C.; Catalina, F.; del Monte, F.; Ferrer, M. L. *Chem. Mater.* **2007**, *19*, 1968.
(50) (a) Hecht, V.; Langer, O.; Deckwer, W. D. *Biotechnol. Bioeng.* **2000**, *70*, 391. (b) Pekdemir, T.; Keskinler, B.; Yildiz, E.; Akay, G. *J. Chem. Technol. Biotechnol.* **2003**, *78*, 773. (c) Giorno, L.; Drioli, E. *TIBTECH* **2000**, *18*, 339. (d) Erhan, E.; Keskinler, B.; Akay, G.; Algur, O. F. *J. Membr. Sci.* **2002**, *206*, 361. (e) Kwak, M. Y.; Rhee, J. S. *Biotechnol. Bioeng.* **1992**, *39*, 903.
(51) (a) Ishige, T.; Honda, K.; Shimizu, S. *Curr. Opin. Chem. Biol.* **2005**, *9*, 174. (b) White, C.; Sharman, A. K.; Gadd, G. M. *Nat. Biotechnol.* **1998**, *16*, 572. (c) Schmid, A.; Dordick, J. S.; Hauer, B.; Kiener, A.; Wubbolts, M.; Witholt, B. *Nature (London)* **2001**, *409*, 258.
(52) Hollister, J. A. *Nat. Mater.* **2005**, *4*, 518.
(53) Soltmann, U.; Böttcher, H.; Koch, D.; Grathwohl, G. *Mater. Lett.* **2003**, *57*, 2861.
(54) Deville, S.; Saiz, E.; Ravi, K.; Nalla, R. V.; Tomsia, A. P. *Science* **2006**, *311*, 515.
(55) An, Y. H. In *Mechanical Testing of Bone and the Bone-Implant Interface*; CRC Press: Boca Raton, FL, 2000; pp 41–63.
(56) Gutierrez, M. C.; Hortigüela, M. J.; Amarilla, J. M.; Jimenez, R.; Ferrer, M. L.; del Monte, F. *J. Phys. Chem. C* **2007**, *111*, 5557.
(57) Bryning, M. B.; Milkie, D. E.; Islam, M. F.; Hough, L. A.; Kikkawa, J. M.; Yodh, A. G. *Adv. Mater.* **2007**, *19*, 661–664.
(58) Cao, A.; Dickrell, P. L.; Sawyer, W. G.; Ghasemi-Nejhad, M. N.; Ajayan, P. M. *Science* **2005**, *310*, 1307.
(59) (a) Xu, Y.-Q.; Flor, E.; Kim, M. J.; Hamadani, B.; Schmidt, H.; Smalley, R. E.; Hauge, R. H. *J. Am. Chem. Soc.* **2006**, *128*, 6560. (b) Jung, Y. J.; Kar, S.; Talapatra, S.; Soldano, C.; Viswanathan, G.; Li, X.; Yao, Z.; Ou, F. S.; Avadhanula, A.; Vajtai, R.; Curran, S.; Nalamasu, O.; Ajayan, P. M. *Nano Lett.* **2006**, *6*, 413.
(60) Duggal, R.; Hussain, F.; Pasquali, M. *Adv. Mater.* **2006**, *18*, 29.
(61) Dalton, A. B.; Collins, S.; Muñoz, E.; Razal, J. M.; Ebron, V. H.; Ferraris, J. P.; Coleman, J. N.; Kim, B. G.; Baughman, R. H. *Nature (London)* **2003**, *423*, 703.
(62) Wei, D.; Liu, Y.; Cao, L.; Fu, L.; Li, X.; Wang, Y.; Yu, G.; Zhu, D. *Nano Lett.* **2006**, *6*, 186.
(63) Schröder, U.; Nieben, J.; Scholz, F. *Angew. Chem., Int. Ed.* **2003**, *42*, 2880.
(64) Chaudhuri, S. K.; Lovley, D. R. *Nat. Biotechnol.* **2003**, *21*, 1229.
(65) Liu, H.; Li, S.; Zhai, J.; Li, H.; Zheng, Q.; Jiang, L.; Zhu, D. *Angew. Chem., Int. Ed.* **2004**, *43*, 1146.
(66) Gutierrez, M. C.; Garcia-Carvajal, Z. Y.; Hortigüela, M. J.; Yuste, L.; Rojo, F.; Ferrer, M. L.; del Monte, F. *J. Mater. Chem.* **2007**, *17*, 2992.
(67) (a) Sun, Y.; Fu, K.; Lin, Y.; Huang, W. *Acc. Chem. Res.* **2002**, *35*, 1096. (b) Jia, G.; Wang, H.; Yan, L.; Wang, X.; Pei, R.; Yan, T. *Environ. Sci. Technol.* **2005**, *39*, 1378–83.
(68) (a) Hu, H.; Ni, Y.; Montana, V.; Haddon, R. C.; Parpura, V. *Nano Lett.* **2004**, *4*, 507–11. (b) Hu, H.; Ni, Y.; Mandal, S. K.; Montana, V.; Zhao, B.; Haddon, R. C.; Parpura, V. *J. Phys. Chem. B* **2005**, *109*, 4285–89.
(69) Abarrategui, A.; Gutierrez, M. C.; Hortigüela, M. J.; Ramos, V.; Lopez-Lacomba, J. L.; Ferrer, M. L.; del Monte, F. *Biomaterials* **2008**, *29*, 94–102.
(70) Dujardin, E.; Ebbesen, T. W.; Krishnan, A.; Treacy, M. M. J. *Adv. Mater.* **1998**, *10*, 611–613.
(71) Ebbesen, T. W. *Carbon Nanotubes: Preparation and Properties*; CRC Press: Boca Raton, FL, 1997.
(72) Lam, C. W.; James, J. T.; McCluskey, R.; Hunter, R. L. *Toxicol. Sci.* **2004**, *77*, 126–134.
(73) Lundborg, M.; Johard, U.; Lastbom, L.; Gerde, P.; Camner, P. *Environ. Res.* **2001**, *86*, 244–253.
(74) Reynolds, C. H.; Annan, N.; Beshah, K.; Huber, J. H.; Shaber, S. H.; Lenkinski, R. E.; Wortman, J. A. *J. Am. Chem. Soc.* **2000**, *122*, 8940–5.
(75) Gutierrez, M. C.; Garcia-Carvajal, Jobbagy, M.; Rubio, F.; Ferrer, M. L.; del Monte, F. *Adv. Funct. Mater.* **2007**, *17*, 3505–3513.
(76) Crumplin, G. C. *Int. Congr. Symp. Ser.—R. Soc. Med.* **1986**, *104*, 1.
(77) Choi, S. H.; Kwon, J.-H.; Kim, C.-W. *Biosci. Biotechnol. Biochem.* **2004**, *68*, 749.
(78) Williams, E.; Angell, C. A. *J. Phys. Chem.* **1977**, *81*, 232.
(79) Velikov, V.; Borick, S.; Angell, C. A. *Science* **2001**, *294*, 2335.
(80) Gutierrez, M. C.; Jobbagy, M.; Ferrer, M. L.; del Monte, F. *Chem. Mater.* (DOI 10.1021/cm7020164).
(81) Araki, K.; Halloran, J. W. *J. Am. Ceram. Soc.* **2005**, *88*, 1108.
(82) (a) Yoon, B.-H.; Koh, Y.-H.; Park, C.-S.; Kim, H.-E. *J. Am. Ceram. Soc.* **2007**, *90*, 1744. (b) Koh, Y.-H.; Song, J.-H.; Lee, E.-J.; Kim, H.-E. *J. Am. Ceram. Soc.* **2006**, *89*, 3089–3093. (c) Yoon, B.-H.; Lee, E.-J.; Kim, H.-E.; Koh, Y.-H. *J. Am. Ceram. Soc.* **2007**, *90*, 1753.
(83) Zhang, H.; Long, J.; Cooper, A. I. *J. Am. Chem. Soc.* **2005**, *127*, 13482.
(84) (a) McCann, J. T.; Marquez, M.; Xia, Y. *J. Am. Chem. Soc.* **2006**, *128*, 1436. (b) Im, S. H.; Jeong, U.; Xia, Y. *Nat. Mater.* **2005**, *4*, 671.

CM702028Z